Chemical Geology 564 (2021) 120053

Contents lists available at ScienceDirect

Chemical Geology

journal homepage: www.elsevier.com/locate/chemgeo

Osmium isotopic constraints on sulphide formation in the epithermal environment of magmatic-hydrothermal mineral deposits

Nicolas J. Saintilan [a,b,j,*], Adam D. Sproson [a,k], David Selby [a,c], Bertrand Rottier [d,e,1], Vincent Casanova [f,1], Robert A. Creaser [b], Kalin Kouzmanov [f], Lluís Fontboté [f], Matthias Piecha [g], Manfred Gereke [h], James J. Zambito IV [i]

[a] Department of Earth Sciences, University of Durham, Durham DH1 3LE, United Kingdom
[b] Department of Earth and Atmospheric Sciences, University of Alberta, Edmonton, Alberta T6G 2E3, Canada
[c] State Key Laboratory of Geological Processes and Mineral Resources, School of Earth Resources, China University of Geosciences, Wuhan, China
[d] Département de Géologie et Génie Géologique, Université Laval, Québec, Canada
[e] Centre de recherche sur la géologie et l'ingénierie des ressources minérales (E4m), Québec, Canada
[f] Department of Earth Sciences, University of Geneva, Rue des Maraîchers, 1205 Geneva, Switzerland
[g] Geologischer Dienst NRW – Landesbetrieb, De-Greiff-Str. 195, 47803 Krefeld, Germany
[h] Hopfengarten 6, 35085 Mölln, Germany
[i] Beloit College, Department of Geology, 700 College Street, Beloit, WI 53511, USA
[j] Institute of Geochemistry and Petrology, Department of Earth Sciences, ETH Zürich, Clausiusstraße 25, 8092 Zürich, Switzerland
[k] Atmosphere and Ocean Research Institute, The University of Tokyo, 5-1-5 Kashiwa-no-ha, Kashiwa 275-8564, Japan

ARTICLE INFO

Editor: Prof. Donald Dingwell

Keywords:
Enargite
Pyrite
Metal tracer
Devonian
Shale

ABSTRACT

In the magmatic-hydrothermal environment, fluids with similar metal concentrations and sources may yield contrasting mineral assemblages in successive stages of sulphide mineralization. These differences are linked to the physico-chemical conditions of the mineralizing fluids (e.g., T, pH, fS_2, fO_2) acquired during their interaction with country rocks and/or by mixing with groundwater. Here, we integrate petrography and osmium (Os) isotope ($^{187}Os/^{188}Os$) sulphide geochemistry, and discuss novel constraints on magmatic fluid-rock interaction and magmatic fluid-groundwater mixing that are deemed to govern sulphide deposition in magmatic-hydrothermal systems. We studied pyrite (FeS_2) and enargite (Cu_3AsS_4) from the porphyry-related polymetallic Cerro de Pasco (14.54–14.41 Ma) and Colquijirca (10.83–10.56 Ma) epithermal deposits in the Central Andes, Peru. Sulphide mineralization is genetically associated with Miocene magmatism and includes breccia and replacement bodies of carbonate country rocks, and veins cutting the magmatic and sedimentary country rocks.

At both deposits, pyrite is followed by enargite in the paragenesis. Pyrite has a radiogenic initial $^{187}Os/^{188}Os$ isotopic composition ($^{187}Os/^{188}Os_{i\text{-}pyrite}$ or $Os_{i\text{-}pyrite}$ = 0.80 to 1.45). Enargite (I) enclosing pyrite or filling in cracks in pyrite also has a radiogenic initial $^{187}Os/^{188}Os$ isotopic composition ($Os_{i\text{-}enargite\ I}$ = 0.56 to 1.24). Conversely, enargite (II) that formed on irregular surfaces on earlier pyrite has an unradiogenic $^{187}Os/^{188}Os$ isotopic composition ($Os_{i\text{-}enargite\ II}$ = 0.13 to 0.17). Our data show that the paragenetic evolution from pyrite to enargite records a sharp change in the osmium isotope composition within these sulphides.

Pyrite and enargite (I) record radiogenic initial $^{187}Os/^{188}Os$ isotopic compositions, indicating interaction of magmatic hydrothermal fluids with the sedimentary country rocks. However, the unradiogenic initial $^{187}Os/^{188}Os$ isotopic composition of enargite (II) suggests that magmatic fluids with a mantle-like $^{187}Os/^{188}Os$ signature ascended from parental magmatic chambers to the epithermal environment without incorporation of crustal Os via fluid-rock interaction or mixing with groundwater. This difference may be due to the country rocks being altered during previous stages, with the radiogenic crustal Os signature being flushed by earlier magmatic pulses. Our findings imply that ore metals (i.e., Cu, Au) are magma-derived, whereas the Os isotopic composition of pyrite and some enargite in epithermal deposits may capture the signature of the interaction of magmatic fluids with country rock lithologies (e.g., the Eifelian black shale in the study area) and/or groundwater. Thus,

* Corresponding author at: Institute of Geochemistry and Petrology, Department of Earth Sciences, ETH Zürich, Clausiusstraße 25, 8092 Zürich, Switzerland.
E-mail address: nicolas.saintilan@erdw.ethz.ch (N.J. Saintilan).
[1] These authors contributed equally to the work.

https://doi.org/10.1016/j.chemgeo.2020.120053
Received 10 August 2020; Received in revised form 28 December 2020; Accepted 31 December 2020
Available online 14 January 2021

the isotopic composition of the siderophile and chalcophile trace element Os in sulphides may act as a tracer of metal source, and degree of wall-rock interaction.

1. Introduction

The circulation of magmatic-hydrothermal and basinal hydrothermal fluids contributes to large metal fluxes in the continental crust (Simmons et al., 2005; Wilkinson et al., 2009; Richards, 2011). Anomalous metal concentrations typically occur where metal-bearing

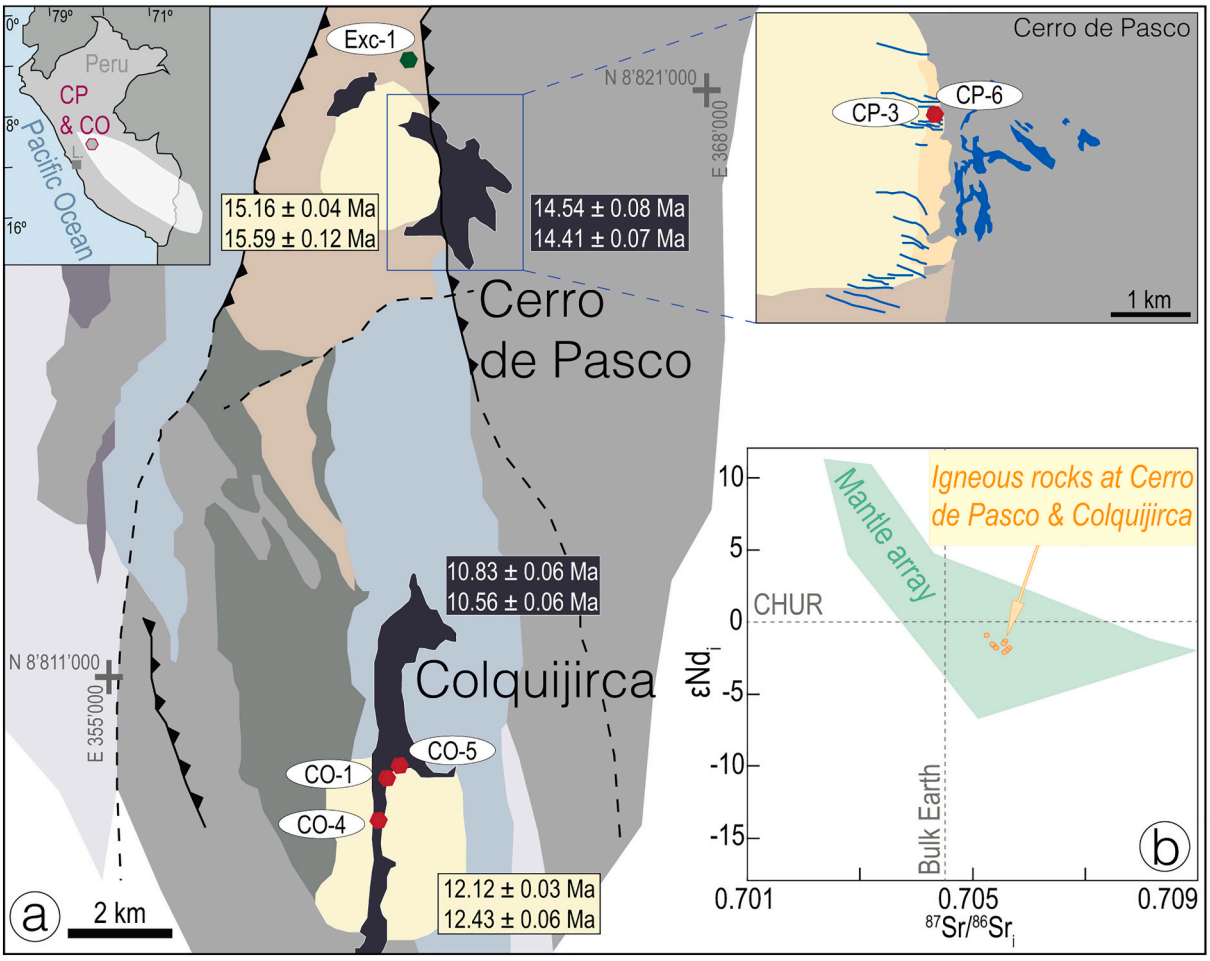

Legend to Figure 1a

- Quaternary cover
- Miocene diatreme & dome complex
- Eocene limestone and marl
- Cretaceous sandstone
- Lower Jurassic to Upper Triassic limestone and dolostone
- Permian–Triassic sandstone
- Devonian shale and phyllite
- Enargite-pyrite sample
- Shale sample
- Cu-Ag-Au-Zn-Pb enargite-pyrite vein
- Replacement-type polymetallic mineralization (Zn-Pb-Ag-Bi-Cu)
- Pyrite-quartz body
- Polymetallic mineralization (vein-type and replacement-type)
- Thrust and reverse fault
- Other fault

Fig. 1. a. Geological map of the district hosting the Cerro de Pasco and Colquijirca mineral deposits in Central Peru. Inset shows the geographical location of Peru, and the extent of Devonian sedimentary units (white shape; Harrison, 1943; Boucot et al., 1980) across the border between Bolivia and Peru. Ages of mineralization and volcanic rocks after Bendezú et al. (2003, 2008), Baumgartner et al. (2009), Rottier et al. (2020). Note: At Colquijirca, the locations of samples are projected to surface. They were sampled at depth at the contact between the Miocene diatreme and dome complex and the Eocene limestone of the Calera Formation that was intruded by Miocene volcanic and magmatic rocks. b. Sr and Nd initial isotopic composition of volcanic and magmatic rocks at Cerro de Pasco and Colquijirca (data from Rottier, 2016). Abbreviations: CP: Cerro de Pasco; CO: Colquijirca.

gangue and sulphide minerals become saturated and precipitate (Reed and Palandri, 2006), with some of the solutes potentially incorporated by minerals that replace the country rocks. The decrease in the solubility of mineral constituents from an aqueous solution to minerals is influenced by the evolution of the fluid (Audétat et al., 1998; Reed and Palandri, 2006; Kouzmanov and Pokrovski, 2012). In addition, solution composition and the parameters of pressure and temperature that are involved in mineral precipitation are affected by fluid-rock interaction along the fluid path (Seedorff et al., 2008; Steefel and Maher, 2009). In order to decipher the fluid evolution from source to sink and constrain the processes leading to precipitation of sulphide minerals, a variety of studies are conducted, including the determination of mineral paragenesis combined with microthermometry and in situ chemical analyses of individual fluid inclusions of assemblages in both gangue and ore minerals. These investigations provide temperatures of entrapment and the chemical composition of the fluid (e.g., Audétat et al., 1998; Hedenquist and Richards, 1998; Wilkinson et al., 2009; Kouzmanov et al., 2010; Catchpole et al., 2015; Casanova et al., 2018; Ortelli et al., 2018). These studies, together with complementary stable and radiogenic isotope data ($\delta^{18}O$, $\delta^{13}C$, $\delta^{2}H$, $\delta^{34}S$, $^{87}Sr/^{86}Sr$) on gangue and sulphides, contribute information about fluid composition and sources, and fluid-rock interaction (e.g., Bendezú, 2007; Zhai et al., 2018; Marques de Sá et al., 2019).

However, there is evidence that the physico-chemical conditions of gangue and sulphide mineral precipitation are not always the same (Simmons et al., 1988; Roedder and Bodnar, 1997; Wilkinson et al., 2009; Kouzmanov et al., 2010). Thus, complementary methods to directly track the source and evolution of fluids responsible for sulphide precipitation in hydrothermal deposits are required. Here, we utilise the rhenium-osmium (Re-Os) systematics of sulphide minerals to obtain the initial osmium isotope ($^{187}Os/^{188}Os_i$ or Os_i) composition to trace the fluid history – mixing and/or fluid-rock interaction. This methodology can be applied to mineral deposits with debated fluid sources and fluid pathways. We studied the large, Cordilleran, polymetallic, and epithermal deposits at Cerro de Pasco and Colquijirca, central Peru (Fig. 1a), which both formed in magmatic-hydrothermal systems (Baumgartner et al., 2008; Bendezú and Fontboté, 2009; Rottier et al., 2018). These deposits have well-constrained geological and geochronological frameworks, including the physico-chemical characteristics of the fluids responsible for gangue and sulphide mineral precipitation, plus petrographic and isotopic evidence of fluid-rock interaction. Previous studies concluded that the widespread pyrite (FeS_2)-enargite (Cu_3AsS_4) deposition was related to cooling of low-density magmatic fluids, mixing with groundwater, and interaction with country rocks (Bendezú, 2007; Bendezú et al., 2003, 2008; Bendezú and Fontboté, 2009; Baumgartner et al., 2008, 2009; Rottier et al., 2016, 2018). Here, we determined the $^{187}Os/^{188}Os_i$ composition of sulphide and sulphosalts minerals (collectively referred as "sulphides" hereafter) and provide new constraints on fluid interaction and evolution.

2. Case study area

At the Colquijirca and Cerro de Pasco deposits (Fig. 1a), large, polymetallic, and epithermal ore bodies are genetically associated with middle Miocene magmatic intrusion, dacitic lava and sub-volcanic domes (Fig. 1a; from 12.43 ± 0.06 Ma to 12.12 ± 0.03 Ma at Colquijirca, $^{39}Ar/^{40}Ar$ biotite thermochronology, Bendezú et al., 2003; single zircon ID-TIMS U-Pb geochronology, Baumgartner et al., 2009; from 15.59 ± 0.12 to 15.16 ± 0.04 Ma at Cerro de Pasco, single zircon ID-TIMS U-Pb geochronology and molybdenite Re-Os model age; Baumgartner et al., 2009; Rottier et al., 2020). The trace element composition of the Miocene magmatic rocks (high Sm/Yb >4 and low Y/Th <1.5), as well as their position at the base of the mantle array in εNd_i vs. Sr_i space (Fig. 1b; Rottier, 2016; Rottier et al., 2020) argue for limited crustal contamination during emplacement (Bissig et al., 2008; Bissig and Tosdal, 2009). The Miocene volcanic and sub-volcanic rocks at Colquijirca and Cerro de Pasco were emplaced into sedimentary successions that include several 100 s m thick, weakly metamorphosed, organic-rich Devonian shale belonging to the Excelsior Group, Triassic siliciclastic of the Mitu Group, Upper Triassic to Lower Jurassic carbonate units of the Pucará Group, and, at Colquijirca, Eocene limestone and marl (Fig. 1a; Rosas et al., 2007; Baumgartner et al., 2008; Bendezú and Fontboté, 2009; Spikings et al., 2016).

At both deposits, hypogene mineralization follows a similar evolution near the Miocene volcanic edifices and includes several stages that were superimposed in time and space (Einaudi, 1977; Bendezú and Fontboté, 2009; Baumgartner et al., 2008; Rottier et al., 2016, 2018). At Cerro de Pasco, an evolution from low- to intermediate- and high-sulphidation conditions is recognized (Einaudi, 1977; Baumgartner et al., 2008; stages "A", "B" and "C" of Rottier et al., 2016, 2018). Pipes of pyrrhotite with an outer shell of Zn-Pb-Ag mineralization formed at the contact between Miocene volcanic and sub-volcanic rocks and carbonate country rocks (stage A). Quartz and pyrite dominated stage B in the form of deep veins and funnel-shaped massive replacement bodies of both volcanic units and limestone country rocks. Finally, zoned Zn-Pb-Ag-Cu carbonate-replacement bodies and Cu-Ag-Au pyrite-enargite veins and/or carbonate-replacement pods are referred to as stage C_1 and C_2, respectively.

At Colquijirca, the low-sulphidation stage is almost inexistent but an evolution from intermediate- to high-sulphidation conditions is similar to the one observed at Cerro de Pasco (Bendezú and Fontboté, 2009). A widespread barren stage comprises quartz-pyrite replacing surrounding carbonate country rocks and Miocene volcanic and sub-volcanic rocks. The "Main Ore Stage", which largely overprinted the quartz-pyrite replacements, is characterised by well-defined mineralogical zones. The internal zone is composed of enargite ± pyrite ± Cu-As-Sb-Pb-Ag sulphosalts ± Au-Ag tellurides ± quartz. It grades into a zone dominated by Cu-sulphides, pyrite and quartz that passes into a zone dominated by Zn-Pb sulphides intergrown with pyrite and surrounded by Fe-Mn-Zn carbonates and iron oxides.

The enargite and pyrite samples selected for the present study come from comparable high-sulphidation mineral assemblages from "Stage C_2" in Cerro de Pasco (Rottier et al., 2016, 2018) and the "Main Ore Stage" in Colquijirca (Bendezú and Fontboté, 2009). The age of the studied high-sulphidation samples is known from $^{39}Ar/^{40}Ar$ alunite thermochronology (Fig. 1a; Cerro de Pasco, at 14.54 ± 0.08 to 14.41 ± 0.07 Ma, Baumgartner et al., 2009; Colquijirca, at 10.83 ± 0.06 to 10.56 ± 0.06 Ma, Bendezú et al., 2008).

3. Sample selection rationale

3.1. Sample selection from epithermal sulphide mineralization

Five samples containing enargite-pyrite were selected from enargite-pyrite veins and mineralized bodies replacing country rocks at the Colquijirca and Cerro de Pasco epithermal deposits (CO: identification code for Colquijirca, CP: identification code for Cerro de Pasco; Fig. 2, Table 1). In these samples, where both enargite and pyrite are present, enargite postdates pyrite in the paragenetic sequence at both deposits. We distinguish two populations of enargite (enargite I & II) based on textural characteristics. At Colquijirca, centimetric enargite crystals amalgamated to a mass enclosing pyrite (sample CO-4, enargite I). Centimetric enargite crystals postdated minor millimetric quartz crystals and cemented a breccia of silicified carbonate rocks (sample CO-1, enargite I). In addition, euhedral centimetric enargite crystals grew on fracture surface of earlier fine-grained pyrite in a breccia of silicified carbonate rocks (sample CO-5, enargite II). At Cerro de Pasco, samples CP-3 and CP-6 are characteristic examples of the Cu-Ag-Au pyrite-enargite veins of stage C_2 (Baumgartner et al., 2008; Rottier et al., 2016, 2018). These samples come from enargite-pyrite veins that cut across the diatreme breccia (CP-3, enargite II) and older (stage B) barren pyrite-quartz body (CP-6, enargite I). In both samples, pyrite crystallized

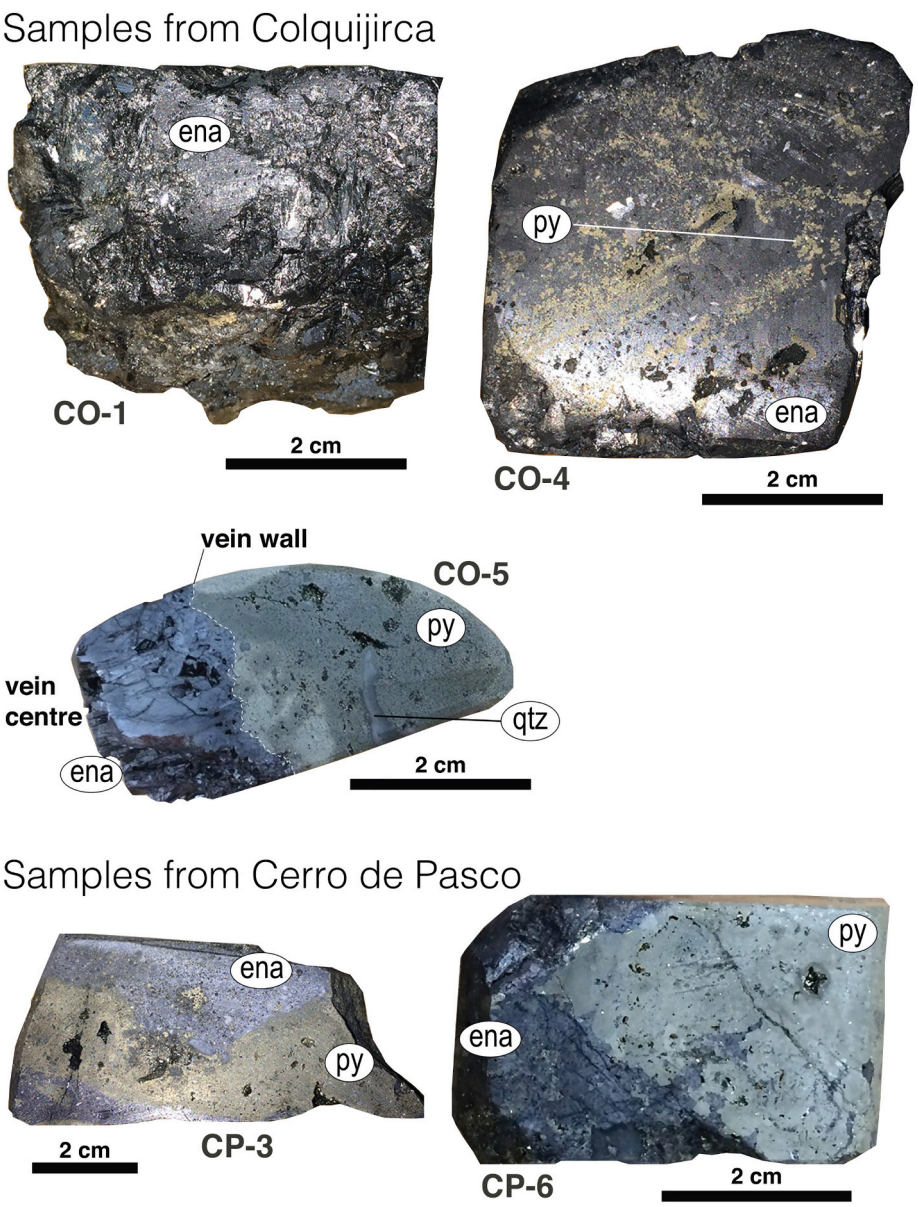

Fig. 2. Enargite-pyrite samples from the Colquijirca and Cerro de Pasco deposits utilised in the present study.

before enargite and enargite formed on surfaces made of irregular pyrite surfaces. Small veinlets (< 1 mm) of pyrite associated with tennantite, sphalerite and galena usually cut across the enargite-pyrite veins. Care was taken to avoid such veinlets in samples CP-3 and CP-6.

3.2. Selection of samples for osmium isotope ($^{187}Os/^{188}Os$) stratigraphy of late Lower Devonian to Middle Devonian shale units

To understand the potential contribution in Os by the country rocks at the time of epithermal mineralization, we analysed the Re-Os composition of a sample of hydrothermally unaltered, weakly metamorphosed organic-rich shale/phyllite in the Excelsior Group from a quarry outside the mineralized area at Cerro de Pasco (Fig. 1a). In the absence of other regionally abundant organic-rich lithologies in the Cerro de Pasco and Colquijirca district, the Excelsior organic-rich shale ought to dominate the Re and Os crustal budget and contribute disproportionally to the Os inventory in the basement of the study area (e.g., Ravizza et al., 1989; Ravizza et al., 1998; Cohen et al., 1999; Selby and Creaser, 2003; Kendall et al., 2009). This organic-rich shale of the Excelsior Group in central Peru belongs to a broad band of outcropping Devonian rocks stretching NW–SE from the Bolivian border to central and northern Peru (inset in Fig. 1a; Harrison, 1943; Boucot et al., 1980). This shale unit is also referred as Cabanillas Group and Concepción Formation in areas to the south areas (Newell, 1949; Boucot et al., 1980; Rodríguez et al., 2011). This sedimentary sequence was deposited in a shallow, warm and marine setting that was open to the ocean (Isaacson, 1975; Boucot et al., 1980). Biogeographic correlations using faunas common to Peru and Colombia constrain the age of shale deposition from late Emsian to Givetian (i.e., ca. 393 to 382 Ma, late Lower Devonian to late Middle Devonian; Boucot et al., 1980; Barrett and Isaacson, 1988; Isaacson and Sablock, 1988; Morzadec et al., 2015; Cohen et al., 2020). Given the open marine environment of deposition of organic-rich shale of the Excelsior Group in Peru (Harrington, 1967; Isaacson, 1975; Boucot et al., 1980), we can look at global equivalents of shale units that were also deposited in open marine setting in the late Lower Devonian to late Middle Devonian. This rationale allows a more comprehensive understanding of the potential range of Os isotopic composition of organic-rich shale in the Excelsior Group at the time of deposition beyond that Os isotopic composition that can be constrained for the quarry sample of Excelsior shale. To this end, we collected five

Table 1
Location, ore stage and mineralogy of the samples utilised in this study.

Deposit	Laboratory sample ID	Mineralization stage	Coordinate system	Easting	Northing	Elevation (m.a.s.l.)	Petrographical and mineralogical description	Mineral phase isolated/ sample ID in Table 2
Colquijirca	CO-1	Main ore stage (Bendezú and Fontboté, 2009)	UTM zone 18S	361,312	8,809,512	4′250	Centimetric enargite crystals in breccia of silicified carbonate rocks. Minor millimetric quartz crystals predate enargite	enargite – CO-1-Ena
Colquijirca	CO-4	Main ore stage (Bendezú and Fontboté, 2009)	UTM zone 18S	360,567	8,807,430	4′067	Massive enargite ore sample composed of centimetric enargite crystals enclosing pyrite	enargite – CO-4-Ena
Colquijirca	CO-5	Main ore stage (Bendezú and Fontboté, 2009)	UTM zone 18S	361,291	8,809,063	4′194	Euhedral centimetric enargite crystals growing in open-space. Enargite postdates fine-grained pyrite in a breccia of silicified carbonate rocks. Some kaolinite (<5 vol%)	pyrite and enargite – CO-5-Py, CO-5-Ena
Cerro de Pasco	CP-3	C_2 (Rottier et al., 2018)	UTM zone 18S	362,208	8,820,494	4′132	Enargite-pyrite veins crosscuting the diatreme breccia	pyrite and enargite – CP-3-Py, CP-3-Ena
Cerro de Pasco	CP-6	C_2 (Rottier et al., 2018)	UTM zone 18S	362,156	8,819,203	4′287	Enargite-pyrite veins crosscuting the pyrite-quartz body	pyrite and enargite – CP-6-Py, CP-6-Ena

Abbreviations: m.a.s.l.: metres above sea level.

samples of Middle Devonian shale units in Germany and the USA (Table 2).

By constraining and using the Re-Os systematics of each shale sample and the known conodont zonation or palaeofauna correspondence for each shale unit, the initial $^{187}Os/^{188}Os$ isotopic composition (Os_i) is estimated for each shale sample at the time of deposition (i.e., osmium isotopic composition acquired from seawater in the depositional environment). Finally, using this representative data set for an estimate of the range of possible initial $^{187}Os/^{188}Os$ isotopic compositions of the entire package of organic-rich shale in the Excelsior Group of Peru, an estimate is calculated for the $^{187}Os/^{188}Os$ isotopic composition in organic-rich shale as the result of the ingrowth of radiogenic $^{187}Os^*$ from the decay of ^{187}Re from the time of deposition in the late Lower Devonian to late Middle Devonian until the timing of epithermal mineralization at Cerro de Pasco and Colquijirca in the Miocene. Finally, by using this approach, we modelled the regional crustal contribution in Os (including radiogenic $^{187}Os^*$) that can potentially be leached from shale in the Excelsior Group.

4. Analytical methods

4.1. Production of monophasic sulphide mineral separates and shale sample preparation

All sulphide-bearing samples were cut into slabs that were thoroughly cleaned using silicon carbide grit, milli-Q water and ethanol to remove any metal traces potentially introduced by hammering or sawing. Samples were cut to facilitate the separation of enargite from pyrite in each sample. The samples were crushed using a zirconia ceramic dish and puck and sieved through disposable nylon sieves to produce 70–200 mesh size fractions. Each 70–200 mesh size fraction was washed with milli-Q water using a drip bottle to create a turbulent flow that would wash the particles finer than 74 μm (200 mesh size). Each fraction was then rinsed with ethanol and dried overnight in an oven at 60 °C. For samples CO-1, CO-4, and CP-3, a Frantz Isodynamic separator was used to produce magnetic (M) and non-magnetic (NM) sub-fractions by applying a 2.2 amp current with 10° side slope and 10° forward slope: 1) pyrite and eventual composite enargite-pyrite grains were collected in the "M2.2 fraction", 2) enargite was collected in the "NM2.2 fraction". Pyrite mineral separates were further purified from eventual quartz and composite grains comprising enargite and pyrite by handpicking under a binocular microscope. For samples CO-5 and CP-6, the quality of the enargite mineral separate from the washed 70–200 mesh size fraction was optimized by handpicking under a binocular microscope.

All shale samples were cut into slabs that were then thoroughly cleaned using silicon carbide grit, Milli-Q water, and ethanol to remove any metal traces potentially introduced by hammering or sawing. The samples were then powdered using a zirconia ceramic dish and puck.

4.2. Sulphide and shale Re-Os isotope geochemistry

For each sulphide analysis, between 270 and 550 mg of pyrite or enargite mineral separate was weighed and transferred into a thick-walled borosilicate Carius tube (Shirey and Walker, 1995). Each sulphide aliquot was dissolved in inverse Aqua Regia (~3 mL of 11 N HCl and ~ 6 mL 16 N HNO_3) with a known amount of $^{185}Re+^{190}Os$ spike solution at 220 °C for 24 h (Laboratory for Sulphide and Source Rock Geochemistry and Geochronology in the Durham Geochemistry Centre, Durham University, UK). The Re-Os laboratory protocol used for sulphides in the present work is described in full in Selby et al. (2009). Each shale sample was dissolved in a Carius tube with ~8 mL of a mixture of $Cr^{VI}O_3$–H_2SO_4 with a known amount of $^{185}Re+^{190}Os$ spike solution at 220 °C for 48 h. The Re-Os laboratory protocol used for shale in the present work further uses Os purification following the solvent extraction (by $CHCl_3$) and microdistillation procedures of Selby and Creaser (2003). Rhenium purification utilised single-bead anion chromatography, following treatment with NaOH and acetone (Selby and Creaser, 2003; Cumming et al., 2012). The Re and Os isotopic compositions of all aliquots were determined by negative thermal ionization mass spectrometry (N-TIMS) using a ThermoScientific Triton mass spectrometer at the Arthur Holmes Laboratory in the Durham Geochemistry Centre, Durham University, UK. Rhenium was measured as ReO_4^- in static mode on Faraday collectors, whereas Os was measured as OsO_3^- in peak-hopping mode on a SEM (Creaser et al., 1991; Völkening et al., 1991). Sulphide and shale measurement quality was monitored by repeated measurements of in-house high purity Re metal standard (125 pg aliquot, $^{185}Re/^{187}Re = 0.59892 \pm 0.00203$, $n = 74$) and *DROsS* [Durham Romil Osmium Standard] Os (50 pg aliquot, $^{187}Os/^{188}Os = 0.160869 \pm 0.000410$, $n = 100$) standard solutions. Total procedural blanks for each set of samples are reported in Tables 2 and 3. The analytical uncertainties result from full error propagation of weighing errors, spike calibration, standard measurements, mass spectrometry analyses and blanks.

Table 2
Summary of the Re-Os data for pyrite and enargite at Colquijirca and Cerro de Pasco.

Deposit	Aliquot	Fraction	Weight	Re	±2σ	Os	±2σ	^{192}Os	± 2σ	^{187}Re/^{188}Os	± 2σ	^{187}Os/^{188}Os	± 2σ	rho	% Re Blank	% ^{187}Os Blank	% ^{188}Os Blank	Os_i at 14.5–14.4 Ma	±2σ	Os_i at 10.8–10.6 Ma	±2σ
			(mg)	(ppb)		(ppt)		(ppt)													
Colquijirca	CO-5-Py-a	hand-picking	513	1.703	0.004	15.1	0.2	5.3	0.1	641	8	1.46	0.03	0.608	0.24	0.54	1.04			1.34	0.07
Colquijirca	CO-5-Py-b	hand-picking	548	1.769	0.004	15.0	0.2	5.3	0.1	669	10	1.53	0.04	0.680	0.26	0.61	1.11			1.41	0.09
Colquijirca	CO-5-Py-c	hand-picking	401	1.562	0.005	13.4	0.1	4.6	0.1	673	9	1.61	0.02	0.784	0.37	0.22	1.74			1.45	0.05
Colquijirca	CO-5-Py-d	hand-picking	400	1.502	0.005	12.6	0.1	4.4	0.1	684	9	1.62	0.03	0.767	0.38	0.23	1.83			1.45	0.05
Colquijirca	CO-1-Ena-a	NM2.2 & hand-picking	473	0.658	0.002	5.4	0.3	1.9	0.2	687	72	1.40	0.27	0.716	0.74	1.90	3.34			1.23	0.44
Colquijirca	CO-1-Ena-b	NM2.2 & hand-picking	434	0.561	0.002	4.7	0.3	1.6	0.2	677	95	1.39	0.21	0.714	0.95	2.39	4.20			1.24	0.60
Colquijirca	CO-4-Ena-a	NM2.2 & hand-picking	496	0.150	0.001	22.9	1.3	8.4	1.1	36	5	1.11	0.21	0.707	3.08	0.52	0.72			1.10	0.51
Colquijirca	CO-4-Ena-b	NM2.2 & hand-picking	435	0.166	0.001	24.4	1.4	9.0	1.2	37	5	1.11	0.21	0.707	3.19	0.55	0.77			1.11	0.51
Colquijirca	CO-5-Ena-a	hand-picking	392	0.193	0.001	673	39	278	37	1.4	0.2	0.13	0.02	0.706	3.03	0.17	0.03			0.13	0.06
Colquijirca	CO-5-Ena-b	hand-picking	416	0.189	0.001	77	4	31	4	12.0	1.6	0.17	0.03	0.703	2.92	1.09	0.23			0.17	0.08
Cerro de Pasco	CP-3-Py-a	M2.2 & hand-picking	386	0.286	0.001	19.9	0.7	7.5	0.6	76	6	0.82	0.09	0.706	2.08	1.00	1.03	0.80	0.23		
Cerro de Pasco	CP-3-Py-b	M2.2 & hand-picking	420	0.523	0.002	24.3	0.6	8.9	0.5	116	6	1.07	0.08	0.706	1.05	0.59	0.80	1.05	0.18		
Cerro de Pasco	CP-3-Py-c	M2.2 & hand-picking	411	0.414	0.001	15.5	0.6	5.7	0.5	144	12	1.05	0.12	0.708	1.35	0.97	1.28	1.01	0.28		
Cerro de Pasco	CP-6-Py-a	hand-picking	425	0.479	0.002	116	3	42	2	22.6	1.1	1.15	0.08	0.706	1.13	0.12	0.17	1.15	0.20		
Cerro de Pasco	CP-6-Py-b	hand-picking	429	0.486	0.002	106	3	38	2	25.3	1.3	1.23	0.09	0.706	1.10	0.12	0.18	1.22	0.21		
Cerro de Pasco	CP-3-Ena-a	NM2.2 & hand-picking	384	0.136	0.005	186	11	76	10	3.5	0.5	0.15	0.03	0.704	4.41	0.53	0.10	0.15	0.07		
Cerro de Pasco	CP-6-Ena-a	hand-picking	297	0.122	0.001	41	4	16	3	15.1	3.0	0.56	0.16	0.705	6.35	0.90	0.63	0.56	0.20		
Cerro de Pasco	CP-6-Ena-b	hand-picking	272	0.130	0.002	22.4	1.9	8.3	1.7	31	6	0.97	0.28	0.707	6.50	1.09	1.33	0.96	0.33		
Cerro de Pasco	CP-6-Ena-c	hand-picking	479	0.187	0.001	24.1	1.4	8.8	1.2	42	6	1.17	0.22	0.707	2.57	0.49	0.72	1.16	0.27		

Blank type	Os (ppt)	± 2σ	^{187}Os/^{188}Os	± 2σ	Re (ppt)	± 2σ
Aqua Regia - $n = 4$	0.08	0.02	0.80	0.06	2.30	0.20

Abbreviations: NMx: non-magnetic at current x amp; M: magnetic at current x amp; Ena: enargite; Py: pyrite.

Table 3
Location and biostratigraphic characteristics of shale samples analysed for Re-Os isotope composition in this study.

Sample	Section	Latitude/ Longitude	Stage	Conodont Zonation	Age of deposition (AoD in Ma)*	Sample weight (g)	Re (ppb)	± 2s	Os (ppt)	± 2s	^{192}Os (ppt)	± 2s	^{187}Re/ ^{188}Os	± 2s	^{187}Os/ ^{188}Os	± 2s	rho	Os_i at AoD	± 2s	Os_i at 14.5–14.4 Ma	± 2s	Os_i at 10.8–10.6 Ma	± 2s
Cargill#17	Cargill #17 core, NY, USA	42°31′22.9"N 76°30′17.5"W	upper Givetian	*Klapperina disparilis*	383.10 to 384.15	1.000	10.610	0.026	282	1	96.1	0.4	219.7	1.0	1.760	0.009	0.584	0.350–0.354	0.011	1.707	0.012	1.72	0.012
ADS14-13	Honert Railway Cut, Germany	51°01′18.88"N 8°25′17.99"E	lower Givetian	*Polygnathus varcus*	386.25 to 386.92	1.001	1.685	0.020	64	1	23.0	0.5	145.9	3.5	1.276	0.037	0.627	0.333–0.334	0.043	1.241	0.047	1.250	0.047
ADS14-12	Honert Railway Cut, Germany	51°01′21.49"N 8°25′17.04"E	upper Eifelian	*Tortodus kock. kockelianus*	388.56 to 388.97	1.017	16.618	0.155	909	11	327.5	6.8	100.9	2.3	1.247	0.036	0.649	0.590–0.591	0.039	1.223	0.045	1.229	0.045
ADS14–10	Limburg Quarry, Germany	51°02′04.14"N 8°23′27.50″E	upper Eifelian	*Tortodus kock. Australis*	388.97 to 389.23	1.001	0.961	0.019	66	1	24.2	1.0	79.0	3.6	1.055	0.060	0.636	0.541–0.541	0.065	1.036	0.075	1.041	0.076
ADS14–4	Sommerseite Quarry, Germany	51°01′19.31"N 8°23′06.27″E	middle Eifelian	*Polygnathus costatus costatus*	389.23 to 391.62	1.003	0.986	0.014	107	2	40.8	1.7	48.1	2.1	0.745	0.043	0.665	0.430–0.432	0.045	0.733	0.053	0.736	0.053
ADS14–4r						1.000	0.990	0.007	94	2	35.7	1.4	55.2	2.3	0.795	0.045	0.699	0.433–0.435	0.047	0.782	0.055	0.785	0.055
NJS_Exc-1	Excelsior Group	10°39′42.70"S 76°16′57.02"W	late Emsian - Givetian	*n/a*	ca. 382 to 393	1.120	0.246	0.004	50.8	0.2	19.5	0.1	25.1	0.4	0.697	0.005	0.196	0.533–0.538	0.012	0.691	0.012	0.693	0.012

*Age of deposition (mega-annum, one million years) based on GTS 2020 age range for the conodont zonation, except for the Excelsior Group. Age of the Excelsior Group is based on the Floresta Fauna of Colombia (see text for details) and the International Stratigraphic Chart GTS 2020.
Os_i at AoD = calculated range in initial $^{187}Os/^{188}Os$ based on the GTS 2020 age range for the conodont zonation.

Blank type	Os (ppt)	± 2σ	$^{187}Os/^{188}Os$	± 2σ	Re (ppt)	± 2σ
Cr-H_2SO_4 − $n = 5$	0.10	0.05	0.21	0.05	16.00	3.00

5. Results

5.1. Re-Os isotope geochemistry of pyrite and enargite

Rhenium and Os contents in pyrite and enargite at both deposits range from 0.1 to 1.8 ppb Re and 4 to 675 ppt Os (Table 2). The initial $^{187}Os/^{188}Os$ isotopic composition of enargite and pyrite aliquots at the time of mineralization (Os_i at *x* Ma; Table 2) is calculated from the Re-Os isotope data as follows: $(^{187}Os/^{188}Os)_i$ or $Os_i = (^{187}Os/^{188}Os)_{measured} - (^{187}Re/^{188}Os_{measured} * (\exp^{(\lambda * t)} - 1))$, where λ is the decay constant of ^{187}Re as determined by Smoliar et al. (1996); $\lambda = 1.666e^{-11} \pm 5.165e^{-14}$ a^{-1}), and *t* is the age of mineralization that is accurately and precisely known at Colquijirca (t_1 = 10.83 ± 0.06 to 10.56 ± 0.06 Ma, Bendezú et al., 2008) and at Cerro de Pasco (t_2 = 14.54 ± 0.08 to 14.41 ± 0.07 Ma, Baumgartner et al., 2009) from $^{39}Ar/^{40}Ar$ alunite thermochronology.

At Colquijirca, the analysed pyrite in the silicified carbonate rock (CO-5-Py: Re = 1.5 to 1.8 ppb, Os = 13 to 15 ppt; Table 2) exhibits a radiogenic initial $^{187}Os/^{188}Os$ isotopic composition (Os_i at 10.8 to 10.6 Ma = 1.34 to 1.45; Fig. 3). Enargite as cement of silicified carbonate country rocks or enclosing earlier pyrite (CO-1-Ena and CO-4-Ena, enargite I: Re = 0.15 to 0.66 ppb, Os = 5 to 24 ppt; Table 2) also has a radiogenic initial $^{187}Os/^{188}Os$ isotopic composition (Os_i at 10.8 to 10.6 Ma = 1.10 to 1.24; Fig. 3), slightly less radiogenic than that of CO-5-Py. In contrast, enargite that grew on fracture surfaces consisting of pyrite (CO-5-Ena-a & b, enargite II: Re = 0.19 ppb, Os = 77 to 673 ppt; Table 2) has an un radiogenic initial $^{187}Os/^{188}Os$ isotopic composition (Os_i at 10.8 to 10.6 Ma = 0.13 to 0.17; Fig. 3).

At Cerro de Pasco, the analysed pyrite predating enargite (CP-3 and CP-6, Fig. 1c; Re = 0.29 to 0.52 ppb, Os = 16 to 116 ppt, Table 1) has a radiogenic initial $^{187}Os/^{188}Os$ isotopic composition (Os_i at 14.5 to 14.4 Ma = 0.80 to 1.22; Fig. 3). Sample CP-6-Ena (enargite (I): Re = 0.12 to 0.19 ppb, Os = 22 to 41 ppt) has a radiogenic initial $^{187}Os/^{188}Os$ isotopic composition (Os_i at 14.5 to 14.4 Ma = 0.56 to 1.16; Fig. 2d) whereas sample CP-3-Ena (enargite (II): Re = 0.14 ppb, Os = 186 ppt) has an unradiogenic initial $^{187}Os/^{188}Os$ isotopic composition (Os_i at 14.5 to 14.4 Ma = 0.15; Fig. 3).

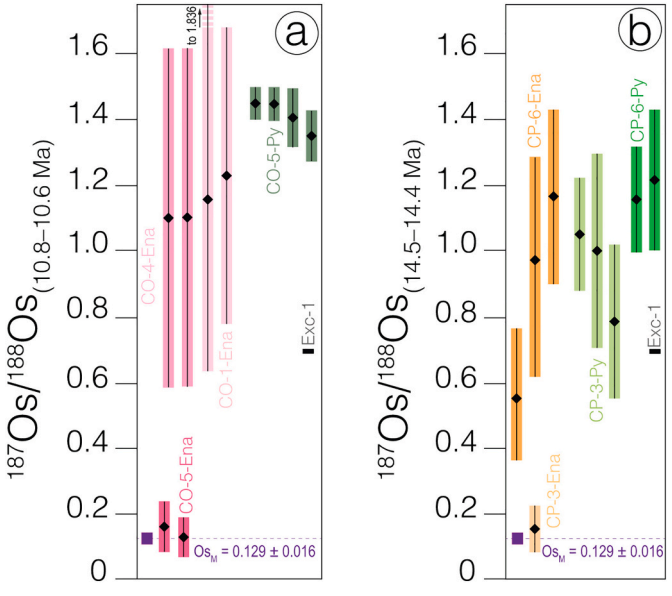

Fig. 3. a. Calculated initial $^{187}Os/^{188}Os$ ratio for enargite and pyrite samples from Colquijirca. b. Calculated initial $^{187}Os/^{188}Os$ ratio for enargite and pyrite samples from Cerro de Pasco. Data point of Excelsior shale is shown in each diagram. See text for discussion.

5.2. Shale Re-Os isotope geochemistry

Two shale samples of lower to upper Givetian age from Germany and the USA have Re abundances between 1.7 and 10.6 ppb with corresponding common Os abundances, expressed as ^{192}Os, of 23 and 96 ppt. Calculated Os_i values for the Givetian shale units overlap within uncertainty (from 0.33 ± 0.04 to 0.35 ± 0.01; Table 3, Fig. 4a). The Re and ^{192}Os contents in three shale samples of middle to upper Eifelian age from Germany are relatively similar (0.96 to 0.99 ppb Re, 24 to 41 ppt ^{192}Os), with the exception of the youngest upper Eifelian sample that is markedly enriched in Re and Os (17 ppb Re and 328 ppt ^{192}Os). Stratigraphic trends in Os_i for the Eifelian shale units are shown in Fig. 4a. The Os_i values for the middle Eifelian aliquots are consistent and reproducible for an individual sample (0.43 to 0.44 ± 0.05, 2σ; Table 3). The Os_i values for the upper Eifelian aliquots are more radiogenic (0.54 ± 0.07 to 0.59 ± 0.04; Table 3).

The shale sample of the Excelsior Group of proposed late Emsian to Givetian age (ca. 393 to 382 Ma) on the basis of biostratigraphic constraints has Re and ^{192}Os abundances of 0.25 ppb and 19.5 ppt, respectively, with an Os_i value of 0.53 to 0.54 ± 0.01. These values overlap within uncertainty with the Os_i values of shale units of the Upper Eifelian age constrained with conodont zonation at ca. 389.23 to 388.56 Ma (Table 3, Fig. 4a).

6. Interpretations and implications

6.1. Potential sources of radiogenic Os in the local crust

Rhenium and Os are incompatible and compatible elements, respectively, during mantle melting (Carlson, 2005). The isobaric decay of ^{187}Re produces radiogenic ^{187}Os at a rate given by the decay constant of ^{187}Re ($\lambda^{187}Re = 1.666e^{-11} \pm 5.165e^{-14}$ a^{-1}, Smoliar et al., 1996). As a result of continental crust generation and its evolution through geological time, the crust has high Re/Os and high radiogenic $^{187}Os/^{188}Os$ ratios (e.g., $^{187}Os/^{188}Os_{crust} = \sim 0.5$ to >> 1; Peucker-Ehrenbrink and Jahn, 2001; Chen et al., 2016) compared to those of the rhenium-depleted primitive upper mantle at any given time in Earth history (Meisel et al., 2001; Carlson, 2005). As outlined above, the trace element, and εNd_i and Sr_i compositions of the Miocene igneous rocks in the study area (Fig. 1b; data from Rottier, 2016) suggest that the associated magmas underwent limited crustal contamination during emplacement (Bissig et al., 2008; Bissig and Tosdal, 2009). Thus, we argue that the exsolved magmatic fluids should have had $^{187}Os/^{188}Os$ ratios close to that of the Miocene primitive upper mantle (Fig. 4b). An $Os_{M\text{-}Miocene}$ value of 0.129 ± 0.016 was calculated for the hypothetical primitive Miocene upper mantle at 14.5 to 10.6 Ma by using present-day values of $^{187}Re/^{188}Os = 0.435 \pm 0.055$ and $^{187}Os/^{188}Os = 0.130 \pm 0.001$ for the primitive upper mantle (Meisel et al., 2001; Carlson, 2005).

As argued above, the organic-rich shale of the Excelsior Group is considered to dominate the Re and Os crustal budget of the country rocks hosting the magmatic-hydrothermal systems at Colquijirca and Cerro de Pasco. Our limited results show that the Excelsior Group shale/phyllite should have had an estimated $^{187}Os/^{188}Os$ composition of ca. 0.69 ± 0.01 at the time of Miocene magmatic activity and magmatic-hydrothermal mineralization between 14.5 and 10.6 Ma (Fig. 4b, Table 3). Furthermore, we show that the Excelsior Group shale has an initial $^{187}Os/^{188}Os$ composition similar to that of other middle to upper Eifelian-age shale that records a distinctly different latitudinal depositional setting (Fig. 4a, Table 3). The Re abundances of organic-rich sedimentary rocks can vary considerably based on stratigraphic position, as can measured post-depositional $^{187}Os/^{188}Os$ compositions (e.g., Rooney et al., 2010). However, in light of the Re-Os data of the middle to upper Eifelian age shale units in Germany, we propose an extended range of possible $^{187}Os/^{188}Os$ compositions, between 0.73 ± 0.05 and 1.23 ± 0.05 for the Excelsior Group at the time of Miocene magmatic-hydrothermal activity (Fig. 4b, Table 3).

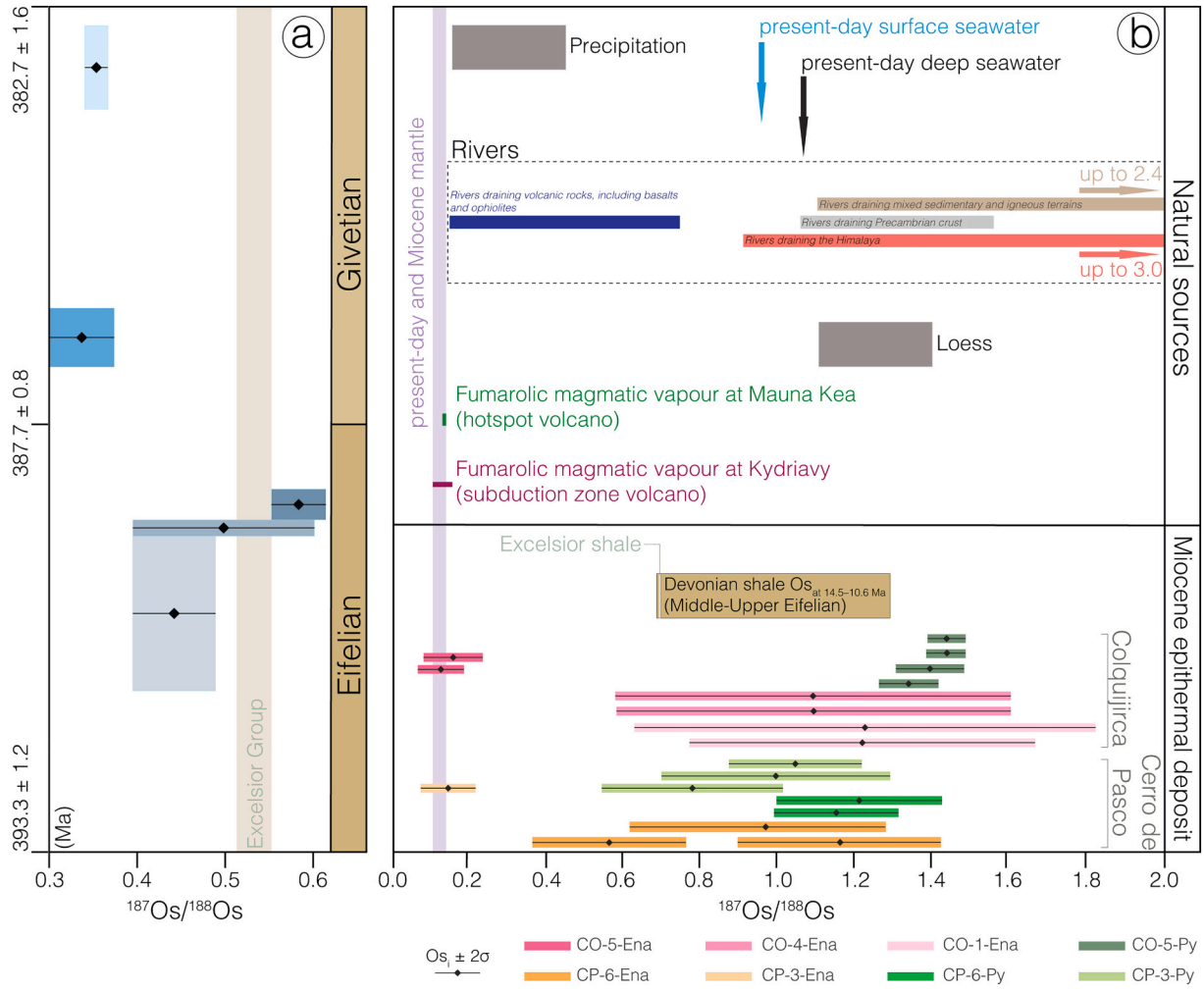

Fig. 4. a. Initial $^{187}Os/^{188}Os$ isotope composition of Devonian shale of established Eifelian and Givetian age analysed in this study. The diagram shows the calculated range of initial $^{187}Os/^{188}Os$ compositions of black shale of the Excelsior Group in Peru for which a broad Eifelian to Givetian age is established. See text for details. b. Model for the various and potential sources of radiogenic crustal Os in the Cerro de Pasco and Colquijirca district. Data references are: precipitation (Chen et al., 2009; Levasseur et al., 1999; Gannoun et al., 2006); seawater (Chen et al., 2009; Levasseur et al., 1998; Sharma et al., 1997; Woodhouse et al., 1999; Martin et al., 2001); rivers (Levasseur et al., 1999; Peucker-Ehrenbrink and Ravizza, 2000; Gannoun et al., 2006; Sproson et al., 2018); magmatic vapours (Lassiter, 2003; Tessalina et al., 2008). Comparison of the $^{187}Os/^{188}Os$ composition of those sources with the initial $^{187}Os/^{188}Os$ composition in pyrite and enargite calculated at the respective time of mineralization at Cerro de Pasco and Colquijirca.

In the study area, ascending magmatic fluids and groundwaters likely interacted with sedimentary country rocks of Devonian to Eocene age. Rhenium and Os have been shown to be potentially mobile through fluid-rock interaction and leaching of black shales in post-depositional times by aqueous fluids; for example, 25 to 64% of the initial budget of Re and 45 to 90% of the initial budget of Os may be lost to aqueous fluids from black shale that exhibit features of weathering and/or crosscutting carbonate veins (Peucker-Ehrenbrink and Hannigan, 2000; Jaffe et al., 2002; Kendall et al., 2009; Georgiev et al., 2012). Thus, black shales contribute significantly to the labile Os inventory of the continental crust (Peucker-Ehrenbrink and Hannigan, 2000).

Water and chemical elements are exchanged between rivers and subsurface reservoirs (Brunner et al., 2017). Rivers may contribute waters with a $^{187}Os/^{188}Os$ composition between 1.2 and up to 2.4 (Peucker-Ehrenbrink and Ravizza, 2000; Peucker-Ehrenbrink and Jahn, 2001) where they drain terrains comprising mixed sedimentary and igneous rocks (e.g., Devonian organic-rich shale, Middle Triassic to Lower Jurassic siliciclastic and carbonate units; Lower Cretaceous carbonaceous shale and coal lenses, and, Lower Cretaceous sandstone with erosive products from the Precambrian Brazilian and Guianan Cratons; Benavides-Cáceres, 1999; Rosas et al., 2007; Scherrenberg et al., 2012; Eocene limestone and marl; Bendezú and Fontboté, 2009).

In conclusion, in the study area, the interaction between magmatic fluids and Devonian shale as well as groundwater may have had the following consequences: (1) the mantle-like $^{187}Os/^{188}Os$ isotopic composition of magmatic fluids may be modified towards more radiogenic $^{187}Os/^{188}Os$ isotope values by addition of radiogenic crustal Os during fluid migration and fluid-rock interaction, and (2) Os dissolved in groundwater will have a radiogenic to highly radiogenic $^{187}Os/^{188}Os$ isotopic composition.

6.2. *Interpretation of the Os isotopic composition of epithermal sulphides*

We envisage that the $^{187}Os/^{188}Os$ composition of pyrite and enargite at the time of mineralization ($Os_{i\text{-}mineral}$) may record, at the mineral scale (and by inference at the deposit scale), the evolution of magmatic-hydrothermal fluids, including fluid-rock interaction and/or mixing with groundwater. At both the Colquijirca and Cerro de Pasco deposits, pyrite-enargite mineralization was preceded by extensive deposition of hydrothermal quartz (Bendezú and Fontboté, 2009; Rottier et al., 2016, 2018). The radiogenic initial $^{187}Os/^{188}Os$ composition of the studied pyrite ($Os_{i\text{-}py}$ = 0.80 to 1.45; Fig. 4b, Table 2) is compatible with a

contribution of radiogenic ^{187}Os from crustal sources. Enargite at both deposits post-dates pyrite in the veins. The initial $^{187}Os/^{188}Os$ composition of enargite has two signatures: (1) radiogenic initial $^{187}Os/^{188}Os$ composition of enargite ($Os_{i\text{-enargite I}} = 0.56$ to 1.24; Fig. 4b, Table 2), and (2) unradiogenic initial $^{187}Os/^{188}Os$ composition of enargite that grew on fracture surface of earlier fine-grained pyrite ($Os_{i\text{-enargite II}} = 0.13$ to 0.17; Fig. 4b, Table 2). Thus, the paragenetic evolution from pyrite to enargite (II) records a sharp change in the osmium isotope composition within these sulphides, i.e., pyrite and enargite (I) with a radiogenic initial $^{187}Os/^{188}Os$ composition identifying a contribution of radiogenic ^{187}Os from crustal sources, versus enargite (II) having a pristine, unradiogenic, mantle-like, initial $^{187}Os/^{188}Os$ composition.

As proposed above, Miocene magmatic fluids would have had an unradiogenic $^{187}Os/^{188}Os$ isotopic composition equivalent to that of the mantle (ca. $Os_i = 0.13$). Subduction-related volcanoes discharge magmatic vapours from fumaroles that contain Re and Os (e.g., 6.3–8.6 ppb Re and 0.9 ppb Os, Taran et al., 1995; Yudovskaya et al., 2008), and possess an unradiogenic $^{187}Os/^{188}Os$ composition ($Os_i = 0.12$ to 0.15; Tessalina et al., 2008). Thus, in the setting of focused magmatic fluid flow in reactivated structures at Cerro de Pasco and Colquijirca (Baumgartner et al., 2008; Bendezú and Fontboté, 2009; Rottier et al., 2018), we propose that magmatic fluids may not interact with wall rocks and capture their crustal radiogenic ^{187}Os (1) if early alteration, including silicification of country rocks, exerts a shielding effect, (2) if magmatic fluids flow through rocks that have suffered previous magmatic fluid-rock interaction, thus eliminating the Os signature of the country rocks.

6.3. *Sulphide osmium isotope composition in the context of the proposed genetic models for the Cerro de Pasco and Colquijirca deposits*

The sharp change from a radiogenic initial $^{187}Os/^{188}Os$ composition for pyrite and enargite (I), to an unradiogenic initial $^{187}Os/^{188}Os$ composition for enargite (II) can be interpreted as follows in the context of the genetic models previously proposed for the Colquijirca and Cerro de Pasco deposits. In line with the conclusions of these studies, our Os isotope data for individual sulphides identify the prominent role of the rock buffer and fluid rock-interaction on sulphide deposition in the epithermal environment of magmatic-hydrothermal systems. Furthermore, the upper end of the highly radiogenic initial $^{187}Os/^{188}Os$ composition of pyrite and enargite (I) (Fig. 4b) is compatible with a contribution in radiogenic ^{187}Os from a highly radiogenic $^{187}Os/^{188}Os$ isotopic composition of groundwater in the study area. Indeed, it is attested that ascending oxidizing magmatic fluids mixed with and were partially diluted by groundwater that contributed to trigger mineralization (Bendezú, 2007; Baumgartner et al., 2008; Bendezú and Fontboté, 2009; Rottier et al., 2018).

In both systems, mineralization involved oxidizing, magmatic fluids. At Cerro de Pasco, in particular, the earliest mineral assemblage is testament of reduced and low-sulphidation conditions close to the pyrite-pyrrhotite boundary. Those conditions were explained by the reduction of early magmatic fluids by country rocks, in particular carbonaceous material present in shale of the Excelsior Group in the basement (Baumgartner et al., 2008; Rottier et al., 2016). In contrast, the stage C_2 at Cerro de Pasco is characterised by acidic and oxidizing conditions typical of high-sulphidation epithermal mineralization (Baumgartner et al., 2008; Rottier et al., 2018). The radiogenic initial $^{187}Os/^{188}Os$ composition of pyrite and enargite I is compatible with leaching and incorporation of radiogenic ^{187}Os along fluid pathways in Devonian shale. Thus, those sulphides with a radiogenic initial $^{187}Os/^{188}Os$ composition resulted from the magmatic, acidic and oxidizing fluids undergoing wall-rock interaction. Conversely, the unradiogenic initial $^{187}Os/^{188}Os$ composition of enargite (II) suggests that, locally, new pulses of magmatic fluid through probably the same channels did not interact with the altered basement rocks (mainly the organic-rich shale of the Excelsior Group) because (1) earlier magmatic fluids had leached and exhausted the crustal radiogenic Os signature of the rock buffer, and/or (2) early alteration including silicification could have insulated the later magmatic fluid from interaction with the rock buffer (Fig. 5 - Steps 1 & 2).

The shielding effect of silicification might have been more prominent at Colquijirca. Pyrite and enargite I mineralization with radiogenic initial $^{187}Os/^{188}Os$ composition in the "Main Ore Stage" overprinted a previous stage of extensive silicification and pyrite mineralization replacing extensively Eocene limestone (Bendezú and Fontboté, 2009). The advanced argillic alteration patterns associated with the Main Ore Stage formed due to acidic and oxidized magmatic vapours (Bendezú and Fontboté, 2009). The pulses of magmatic fluids responsible for the Main Ore Stage, which ascended along fractures through horizons of Triassic sandstone and Devonian shale at depth (Bendezú and Fontboté, 2009), probably reached epithermal levels where country rocks previously replaced by hydrothermal minerals (including silicification) acted as a casing preventing pristine magmatic fluids from interacting with sources of radiogenic crustal Os, i.e., either the Devonian shale rock buffer or groundwater. Such pristine magmatic fluids were responsible for euhedral enargite (II), which grew on walls of earlier pyrite associated with quartz, and exhibits unradiogenic initial $^{187}Os/^{188}Os$ composition of 0.13 to 0.17 at Colquijirca (Figs. 4b & 5 - Step 3, Table 2).

7. Conclusions

Two discrete $^{187}Os/^{188}Os$ isotopic signatures were identified in pyrite and enargite in single hand samples from two epithermal deposits: (1) a radiogenic $^{187}Os/^{188}Os$ isotopic composition in pyrite and enargite (I); (2) a mantle-like $^{187}Os/^{188}Os$ isotopic composition recorded only in enargite (II) deposited on surfaces of earlier pyrite. Our findings have two implications:

- o if only pyrite and/or enargite (I) had been analysed in these deposits, the mantle-like $^{187}Os/^{188}Os$ isotopic signature of enargite (II) would not have been identified and it could have been incorrectly concluded that the ore sulphides had only a crustal $^{187}Os/^{188}Os$ signature. Thus, in magmatic-hydrothermal systems where the Re-Os systematics of sulphides remain undisturbed, Re-Os isotope geochemistry of individual sulphide species in the paragenetic sequence is necessary to identify the origin of fluids, and by inference metals;
- o The $^{187}Os/^{188}Os$ isotopic compositions in pyrite and enargite are compatible with distinct and evolving fluid pathways for the ascent of magmatic fluids during sulphide precipitation in the epithermal environment. In the early stages, in their rise from parental magma chambers to the epithermal environment, magmatic fluids with mantle-like $^{187}Os/^{188}Os$ signature more readily incorporate radiogenic, crustal ^{187}Os via fluid-rock interaction or mixing with groundwater. In following stages, with decreasing buffer capacity and shielding of fluid pathways by previous hydrothermal minerals, new pulses of magmatic fluids may preserve their mantle-like $^{187}Os/^{188}Os$ isotopic signature.

Authors contribution

N.J.S., R.A.C., and D.S. designed the study. N.J.S. carried out petrographic observations, mineral separation, and sulphide Re-Os isotope geochemistry procedures and mass spectrometry analyses. A. D.S., N.J.S. and D.S. carried out shale Re-Os isotope geochemistry procedures and mass spectrometry analyses. B.R. and V.C. selected and provided the sulphide samples. B.R. and V.C. together with K.K. and L.F. provided detailed background on mineralization processes at Colquijirca and Cerro de Pasco and the wider study area. N.J.S., A.D.S. and D.S. interpreted the data. N.J.S. wrote the manuscript with substantial comments by D.S and B.R., and additional comments by V.C., R.A.C, K. K., L.F., A.D.S., and J.J.Z. M.G., M.P. and J.J.Z. provided access to shale

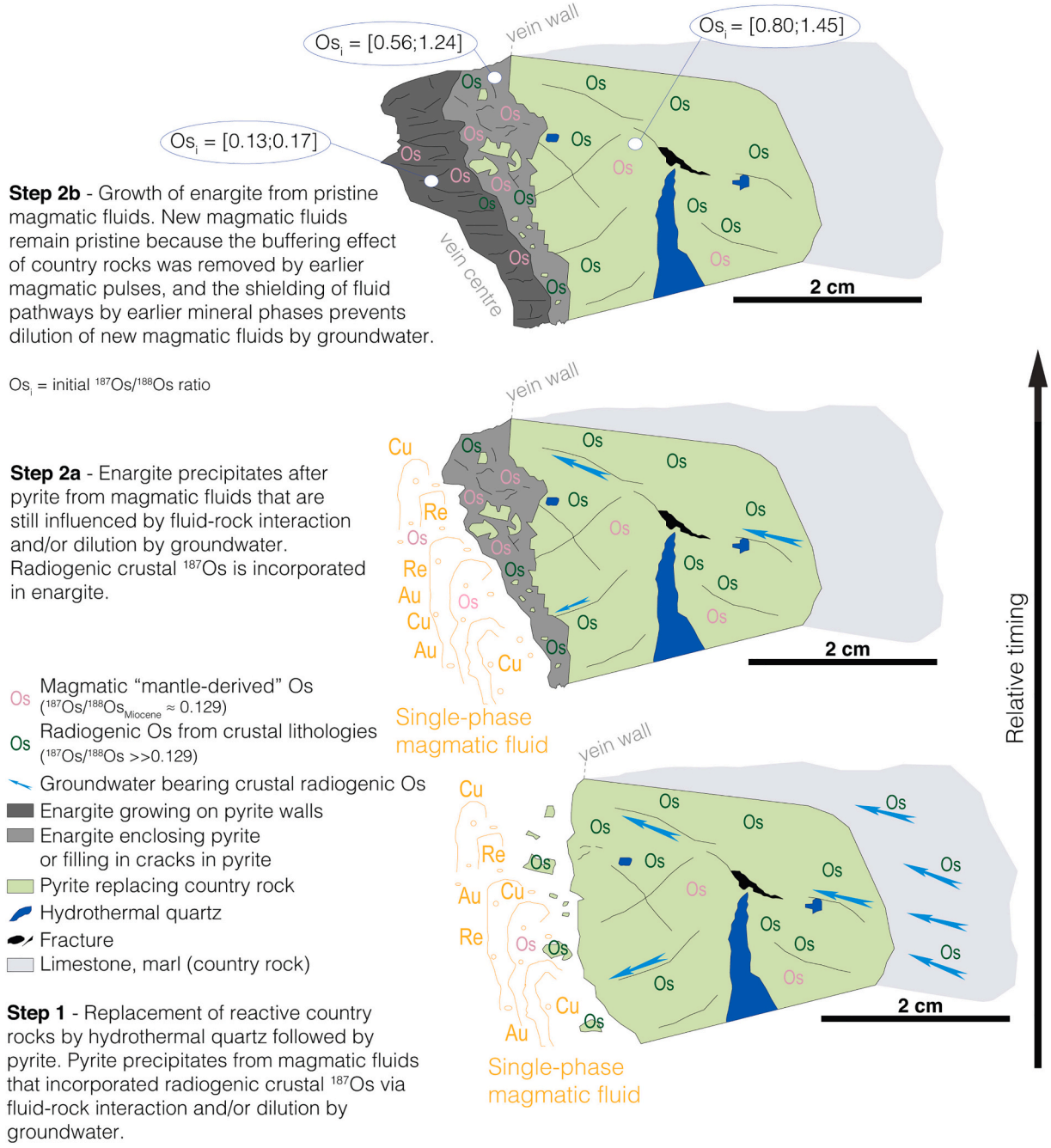

Fig. 5. Model for the evolution of magmatic fluids via fluid-rock interaction and mixing with groundwater through successive stages of pyrite and enargite mineralization characterised by their initial $^{187}Os/^{188}Os$ composition in the present study.

samples in Germany and the USA.

Declaration of Competing Interest

The authors declare that they have no known competing financial interests or personal relationships that could have appeared to influence the work reported in this paper.

Acknowledgments

This work was supported by the Swiss National Science Foundation through Early and Advanced Postdoctoral Mobility Grants (#P2GEP2_162075 & #P300P2_171496) awarded to N.J.S. D.S. acknowledges the TOTAL Endowment Fund and Dida Scholarship of CUG Wuhan. N.J.S., A.D.S., and D.S. are indebted to Dr. Geoff Nowell, Dr. Chris Ottley and Antonia Hoffman for technical support at Durham University. We particularly thank J.W. Hedenquist for his thorough and highly constructive review. The contribution by an anonymous reviewer is also acknowledged. Editor B. Kamber ensured excellent editorial handling.

References

Audétat, A., Günther, D., Heinrich, C.A., 1998. Formation of a magmatic-hydrothermal ore deposit: Insights with LA-ICP-MS analysis of fluid inclusions. Science 279, 2091–2094.

Barrett, S.F., Isaacson, P.E., 1988. Devonian paleogeography of South America, 14. Canadian Society of Petroleum Geologists. Memoir.

Baumgartner, R., Fontboté, L., Vennemann, T., 2008. Mineral zoning and geochemistry of epithermal polymetallic Zn-Pb-Ag-Cu-Bi mineralization at Cerro de Pasco, Peru. Econ. Geol. 103, 493–537.

Baumgartner, R., Fontboté, L., Spikings, R., Ovtcharova, M., Schaltegger, U., Schneider, J., Page, L., Gutjahr, M., 2009. Bracketing the age of magmatic-hydrothermal activity at the Cerro de Pasco epithermal polymetallic deposit, Central Peru: a U-Pb and $^{40}Ar/^{39}Ar$ study. Econ. Geol. 104, 479–504.

Benavides-Cáceres, V., 1999. Orogenic evolution of the Peruvian Andes: the Andean cycle. Geology and Ore Deposits of the Central Andes. Society of Economic Geologists, pp. 61–107. Special Publication 7.

Bendezú, R., 2007. Shallow polymetallic and precious metal mineralization associated with a Miocene diatreme-dome complex: The Colquijirca district of the Peruvian Andes, Geneva, Switzerland, University of Geneva, Terre & Environnement. PhD thesis, 64, p. 221.

Bendezú, R., Fontboté, L., 2009. Cordilleran epithermal Cu-Zn-Pb-(Au-Ag) mineralization in the Colquijirca district, Central Peru: deposit-scale mineralogical patterns. Econ. Geol. 104, 905–944.

Bendezú, R., Fontboté, L., Cosca, M., 2003. Relative age of Cordilleran base metal lode and replacement deposits, and high sulfidation Au-(Ag) epithermal mineralization in the Colquijirca mining district, central Peru. Mineral. Deposita 38, 683–694.

Bendezú, R., Page, L., Spikings, R., Pecskay, Z., Fontboté, L., 2008. New $^{40}Ar/^{39}Ar$ alunite ages from the Colquijirca district, Peru: evidence of a long period of magmatic SO_2 degassing during formation of epithermal Au-Ag and Cordilleran polymetallic ores. Mineral. Deposita 43, 777–789.

Bissig, T., Tosdal, R.M., 2009. Petrogenetic and metallogenetic relationships in the Eastern Cordillera Occidental of Central Peru. J. Geol. 117, 499–518.

Bissig, T., Ullrich, T.D., Tosdal, R.M., Friedman, R., Ebert, S., 2008. The time-space distribution of Eocene to Miocene magmatism in the central Peruvian polymetallic province and its metallogenetic implications. J. S. Am. Earth Sci. 26, 16–35.

Boucot, A.J., Isaacson, P.E., Laubacher, G., 1980. An early Devonian, Eastern Americas Realm Faunule from the coast of southern Peru. J. Paleontol. 54, 359–365.

Brunner, P., Therrien, R., Renard, P., Simmons, C.T., Hendricks Franssen, H.-J., 2017. Advances in understanding river-groundwater interactions. Rev. Geophys. 55, 818–854.

Carlson, R.W., 2005. Application of the Pt-Re-Os isotopic systems to mantle geochemistry and geochronology. Lithos 82, 249–272.

Casanova, V., Kouzmanov, K., Audétat, A., Wälle, M., Ubrig, N., Ortelli, M., Fontboté, L., 2018. Fluid inclusion studies in opaque minerals: II. A comparative study of syngenetic synthetic fluid inclusions hosted in quartz and opaque minerals. Econ. Geol. 113, 1861–1883.

Catchpole, H., Kouzmanov, K., Putlitz, B., Seo, J.H., Fontboté, L., 2015. Zoned base metal mineralization in a porphyry system: Origin and evolution of mineralizing fluids in the Morococha district, Peru. Econ. Geol. 110, 39–71.

Chen, C., Sedwick, P.N., Sharma, M., 2009. Anthropogenic osmium in rain and snow reveals global-scale atmospheric contamination. Proc. Natl. Acad. Sci. 106, 7724–7728.

Chen, K., Walker, R.J., Rudnick, R.L., Gao, S., Gaschnig, R.M., Puchtel, I.S., Tang, M., Hu, Z.C., 2016. Platinum-group element abundances and Re-Os isotopic systematics of the upper continental crust through time: evidence from glacial diamictites. Geochim. Cosmochim. Acta 191, 1–16.

Cohen, A.S., Coe, A.L., Bartlett, J.M., Hawkesworth, C.J., 1999. Precise Re-Os ages of organic-rich mudrocks and the Os isotopic composition of Jurassic seawater. Earth Planet. Sci. Lett. 167, 159–173.

Cohen, K.M., Harper, D.A.T., Gibbard, P.L., Fan, J.-X., 2020. International Commission on Stratigraphy, updated from Cohen, K.M., Finney, S.C., Gibbard, P.L., Fan, J.-X., 2013, The ICS International Stratigraphic Chart. Episodes 36, 199–204.

Creaser, R.A., Papanastassiou, D.A., Wasserburg, G.J., 1991. Negative thermal ion mass spectrometry of osmium, rhenium and iridium. Geochim. Cosmochim. Acta 55, 397–401.

Cumming, V.M., Selby, D., Lillis, P.G., 2012. Re-Os geochronology of the lacustrine Green River Formation: Insights into direct depositional dating of lacustrine successions, Re-Os systematics and paleocontinental weathering. Earth Planet. Sci. Lett. 359-360, 194–205.

Einaudi, M.T., 1977. Environment of ore deposition at Cerro de Pasco, Peru. Econ. Geol. 72, 893–924.

Gannoun, A., Burton, K.W., Vigier, N., Gíslason, S.R., Rogers, N., Mokadem, F., Sigfússon, B., 2006. The influence of weathering process on rivering osmium isotopes in a basaltic terrain. Earth Planet. Sci. Lett. 243, 732–748.

Georgiev, S., Stein, H.J., Hannah, J.L., Weiss, H.M., Bingen, B., Xu, G., Rein, E., Hatløy, V., Løseth, H., Nali, M., Piasecki, S., 2012. Chemical signals for oxidative weathering predict Re-Os isochroneity in black shales, East Greenland. Chem. Geol. 324-325, 108–121.

Harrington, H.J., 1967. Devonian of South America. In: Oswald, D.H. (Ed.), International Symposium on the Devonian system, Calgary, 1, pp. 651–671.

Harrison, J.V., 1943. The geology of the central Andes in part of the Province of Junin, Peru (Final Report). Boletín de la Sociedad Geológica del Peru 16, 7–97.

Hedenquist, J.W., Richards, J.P., 1998. The Influence of geochemical techniques on the development of genetic models for Porphyry Copper Deposits. Rev. Econ. Geol. 10, 238–256.

Isaacson, P.E., 1975. Evidence for a western extracontinental land source during the Devonian period in the Central Andes. Geol. Soc. Am. Bull. 86, 39–46.

Isaacson, P.E., Sablock, P.E., 1988. Devonian system in Bolivia, Peru and Northern Chile. Canadian Society of Petroleum Geologists. Memoir 14.

Jaffe, L.A., Peucker-Ehrenbrink, B., Petsch, S.T., 2002. Mobility of rhenium and organic carbon during black shale weathering. Earth Planet. Sci. Lett. 198, 339–353.

Kendall, B., Creaser, R.A., Gordon, G.W., Anbar, A.D., 2009. Re-Os and Mo isotope systematics of black shales from the Middle Proterozoic Velkerri and Wollogorang Formations, McArthur Basin, northern Australia. Geochim. Cosmochim. Acta 73, 2534–2558.

Kouzmanov, K., Pokrovski, G.S., 2012. Hydrothermal controls on metal distribution in Cu(-Au-Mo) porphyry systems. Society of Economic Geologists Special Publication 16, pp. 573–618.

Kouzmanov, K., Pettke, T., Heinrich, C.A., 2010. Direct analysis of ore-precipitating fluids: combined IR microscopy and LA-ICP-MS study of fluid inclusions in opaque ore minerals. Econ. Geol. 2, 351–373.

Lassiter, J.C., 2003. Rhenium volatility in subaerial lavas: constraints from subaerial and submarine portions of the HSDP-2 Mauna Kea drillcore. Earth Planet. Sci. Lett. 214, 311–325.

Levasseur, S., Birck, J.L., Allegre, C.J., 1998. Direct measurement of femtomoles of osmium and the $^{187}Os/^{186}Os$ ratio in seawater. Science 282, 272–274.

Levasseur, S., Birck, J.L., Allegre, C.J., 1999. The osmium riverine flux and the oceanic mass balance of osmium. Earth Planet. Sci. Lett. 174, 7–23.

Marques de Sá, C., Noronha, F., Cardellach, E., Bobos, I., 2019. Fluid inclusion and (S, C, O, Pb) isotope study of Pb-Zn-(Cu-Ag) hydrothermal veins from Central and Northern Portugal – Metallogenic implications. Ore Geol. Rev. 112, 103043.

Martin, C.E., Peucker-Ehrenbrink, B., Brunskill, G., Szymczak, R., 2001. Osmium isotope geochemistry of a tropical estuary. Geochim. Cosmochim. Acta 63, 1335–1343.

Meisel, T., Walker, R.J., Irving, A.J., Lorand, J.-P., 2001. Osmium isotopic compositions of mantle xenoliths: a global perspective. Geochim. Cosmochim. Acta 65, 1311–1323.

Morzadec, P., Michal, M., Villaroel, C., Janvier, P., Racheboeuf, P.R., 2015. Trilobites and inarticulate brachiopods from the Devonian Floresta Formation of Colombia: a review. Bull. Geosci. 90, 331–358.

Newell, N.D., 1949. Geology of the Lake Titicaca region, Perú and Bolivia. New York. Geological Society of America. Memoir 36. (111 pp.).

Ortelli, M., Kouzmanov, K., Wälle, M., Ubrig, N., Casanova, V., 2018. Fluid inclusion studies in opaque ore minerals: I. Trace element content and physical properties of ore minerals controlling textural features in transmitted near-infrared light microscopy. Econ. Geol. 113, 1845–1860.

Peucker-Ehrenbrink, B., Hannigan, R.E., 2000. Effects of black shale weathering on the mobility of rhenium and platinum group elements. Geology 28, 475–478.

Peucker-Ehrenbrink, B., Jahn, B.-M., 2001. Rhenium-osmium isotope systematics and platinum group element concentrations: Loess and the upper continental crust. Geochem. Geophys. Geosyst. 2 (2001GC000172).

Peucker-Ehrenbrink, B., Ravizza, G., 2000. The marine osmium isotope record. Terra Nova 12, 205–219.

Ravizza, G., Turekian, G.G., Hay, B.J., 1989. Application of the ^{187}Re-^{187}Os system to black shale geochronometry. Geochim. Cosmochim. Acta 53, 3257–3262.

Ravizza, G., Peucker-Ehrenbrink, B., Truit, C.B., 1998. Osmium isotopes as traces of organic matter weathering. Eos. Trans. Am. Geophys. Union 79, 427.

Reed, M.H., Palandri, J., 2006. Sulfide mineral precipitation from hydrothermal fluids. Rev. Mineral. Geochem. 61, 609–631.

Richards, J.P., 2011. Magmatic to hydrothermal metal fluxes in convergent and collided margins. Ore Geol. Rev. 40, 1–26.

Rodríguez, R., Cueva, E., Carlotto, V., 2011. Geología del Cuadrángulo de Cerro de Pasco. INGEMMET, Carta Geológica Nacional (Boletín N° 144 Serie A, escala 1:50,000, 160 p).

Roedder, E., Bodnar, R.J., 1997. Fluid inclusion studies in hydrothermal ore deposits. In: Barnes, H.L. (Ed.), Geochemistry of Hydrothermal Ore Deposits. Wiley, New York, pp. 657–697.

Rooney, A.D., Selby, D., Houzay, J.-P., Renne, P.R., 2010. Re-Os geochronology of a Mesoproterozoic sedimentary succession, Taoudeni basin, Mauritania: Implications for basin-wide correlations and Re-Os organic-rich sediment systematics. Earth Planet. Sci. Lett. 289, 486–496.

Rosas, S., Fontboté, L., Tankard, A., 2007. Tectonic evolution and paleogeography of the Mesozoic Pucará basin, central Peru. J. S. Am. Earth Sci. 26, 16–35.

Rottier, B., 2016. Magmatic and hydrothermal fluid processes at the origin of the giant porphyry-related epithermal polymetallic deposit of Cerro de Pasco (Central Peru). PhD thesis, 2016. University of Geneva, Geneva, Switzerland. no. Sc. 5086.

Rottier, B., Kouzmanov, K., Wälle, M., Bendezú, R., Fontboté, L., 2016. Sulfide replacement processes revealed by textural and LA-ICP-MS trace element analyses: example from the early mineralization stages at Cerro de Pasco, Peru. Econ. Geol. 111, 1347–1367.

Rottier, B., Kouzmanov, K., Casanova, V., Wälle, M., Fontboté, L., 2018. Cyclic dilution of magmatic metal-rich hypersaline fluids by magmatic low-salinity fluid: a major process generating the giant epithermal polymetallic deposit at Cerro de Pasco, Peru. Econ. Geol. 113, 825–856.

Rottier, B., Kouzmanov, K., Ovtcharova, M., Ulianov, A., Wälle, M., Selby, D., Fontboté, L., 2020. Multiple rejuvenation episodes of a silicic magma reservoir at the origin of the large diatreme-dome complex and porphyry-type mineralization events at Cerro de Pasco (Peru). Lithos 376, 105766.

Scherrenberg, A.F., Jacay, J., Holcombe, R.J., Rosenbaum, G., 2012. Stratigraphic variations across the Marañón fold-thrust belt, Peru: implications for the basin architecture of the West Peruvian Trough. J. S. Am. Earth Sci. 38, 147–158.

Seedorff, E., Barton, M.D., Stavast, W.J.A., Maher, D.J., 2008. Root zones of porphyry systems: extending the porphyry model at depth. Econ. Geol. 103, 939–956.

Selby, D., Creaser, R.A., 2003. Re-Os geochronology of organic-rich sediments: an evaluation of organic matter analysis methods. Chem. Geol. 200, 225–240.

Selby, D., Kelley, K.D., Hitzman, M.W., Zieg, J., 2009. Re-Os sulphide (bornite, chalcopyrite, and pyrite) systematics of the carbonate-hosted copper deposits at Ruby Creek, southern Brooks Range, Alaska. Econ. Geol. 104, 437–444.

Sharma, M., Papanastassiou, D.A., Wasserburg, G.J., 1997. The concentration and isotopic composition of osmium in the oceans. Geochim. Cosmochim. Acta 61, 3287–3299.
Shirey, S.B., Walker, R.J., 1995. Carius tube digestion for low-blank rhenium-osmium analysis. Anal. Chem. 67, 2136–2141.
Simmons, S.F., Gemmell, J.B., Sawkins, F.J., 1988. The Santo Nino silver-lead-zinc vein, Fresnillo District, Zacatecas; part II, Physical and chemical nature of ore-forming solutions. Econ. Geol. 83, 1619–1641.
Simmons, S.F., White, N.C., John, D.A., 2005. Geological characteristics of epithermal precious and base metal deposits. In: Society of Economic Geologists, Economic Geology 100th Anniversary Volume, pp. 485–522.
Smoliar, M.I., Walker, R.J., Morgan, J.W., 1996. Re-Os ages of group IIA, IIIA, IVA, and IVB iron meteorites. Science 271, 1099–1102.
Spikings, R., Reitsma, M.J., Boekhout, F., Mišković, A., Ulianov, A., Chiaradia, M., Gerdes, A., Schlategger, U., 2016. Characterization of Triassic rifting in Peru and implications for the early disassembly of western Pangea. Gondwana Res. 35, 124–143.
Sproson, A.D., Selby, D., Gannoun, A., Burton, K.W., Dellinger, M., Lloyd, J.M., 2018. Tracing the impact of coastal water geochemistry on the Re-Os systematics of macroalgae: insights from the basaltic terrain of Iceland. J. Geophys. Res. Biogeosci. 123, 2791–2806.
Steefel, C.I., Maher, K., 2009. Fluid-rock interaction: a reactive transport approach. Rev. Mineral. Geochem. 70, 485–532.
Taran, Y.A., Hedenquist, J.W., Korzhinsky, M.A., Tkachenko, S.I., Shmulovich, K.I., 1995. Geochemistry of magmatic gases from Kudryavy volcano, Iturup, Kuril Islands. Geochim. Cosmochim. Acta 59, 1749–1761.
Tessalina, S.G., Yudovskaya, M.A., Chaplygin, I.V., Birck, J.-L., Capmas, F., 2008. Sources of unique rhenium enrichment in fumaroles and sulphides at Kudryavy volcano. Geochim. Cosmochim. Acta 72, 889–909.
Völkening, J., Walczyk, T., Heumann, K., 1991. Osmium isotopic ratio determination by negative thermal ionization mass spectrometry. Int. J. Spectrometr. Ionic Phys. 105, 147–159.
Wilkinson, J.J., Stoffell, B., Wilkinson, C.C., Jeffries, T.E., Appold, M.S., 2009. Anomalously metal-rich fluids from hydrothermal ore deposits. Science 323, 764–767.
Woodhouse, O.B., Ravizza, G., Kenison-Falkner, K., Statham, P.J., Peucker-Ehrenbrink, B., 1999. Osmium in seawater: vertical profiles of concentration and isotopic composition in the eastern Pacific Ocean. Earth Planet. Sci. Lett. 173, 223–233.
Yudovskaya, M.A., Tessalina, S., Distler, V., Chaplygin, I.V., Chugaev, A.V., Dikov, Y.P., 2008. Behavior of highly-siderophile elements during magma degassing: a case study at the Kudryavy volcano. Chem. Geol. 248, 318–341.
Zhai, D., Liu, J., Tombros, S., Williams-Jones, A.E., 2018. The genesis of the Hashitu porphyry molybdenum deposit, Inner Mongolia, NE China: constraints from mineralogical, fluid inclusion and multiple isotope (H, O, S, Mo, Pb) studies. Mineral. Deposita 53, 377–397.